Journal of Solid State Chemistry **158,** 245–253 (2001)
doi:10.1006/jssc.2001.9099, available online at http://www.idealibrary.com on IDEAL®

A Study of the Magnetic and Thermal Properties of Ln_3RuO_7 (Ln = Sm, Eu)

Daijitsu Harada and Yukio Hinatsu

Division of Chemistry, Graduate School of Science, Hokkaido University, Sapporo 060-0810, Japan

Received September 19, 2000; in revised form December 7, 2000; accepted January 19, 2001; published online April 5, 2001

Crystal structures, and magnetic, electric, and thermal properties of fluorite related compounds Ln_3RuO_7 (Ln = Sm, Eu) have been investigated. For Eu_3RuO_7, a magnetic transition due to Ru^{5+} ions is found at $T_N = 22.5$ K on the susceptibility–temperature curve. Specific heat measurements also exhibit a λ-type anomaly at the same temperature. The Mössbauer spectrum measured at 10 K shows broadening of the line corresponding to magnetic splitting. For Sm_3RuO_7, two magnetic anomalies have been observed at 10.5 and 22.5 K from its magnetic susceptibility measurements. Below 22.5 K Ru^{5+} ions are antiferromagnetically coupled, and when the temperature is decreased through 10.5 K the ordering of Sm^{3+} ions occurs rapidly. Specific heat measurements show first-order transition peaks at $T = 280$ and 190 K for Eu_3RuO_7 and Sm_3RuO_7, respectively. The results of magnetic susceptibility and electric resistivity measurements indicate that these transitions are structural phase transitions.

1. INTRODUCTION

Compounds of composition Ln_3MO_7, where Ln is a lanthanide and M is the 4d or 5d transition metal, have been investigated by several researchers (1–7). For large Ln cations, an orthorhombic fluorite-related superstructure is found, while for the smaller Ln cations, the structure is defect fluorite. Allpress and Rossell (1) pointed out the probable space group $Cmcm$ for La_3NbO_7 and $C222_1$ for Ln_3NbO_7 (Ln = Nd, Gd, Ho, Y). Rossell (2) determined the precise crystal structure of La_3NbO_7 by X-ray powder diffraction and single-crystal electron diffraction experiments. One-third of the La ions are eight-coordinated and lie in rows in the [001] direction which alternate with parallel rows of corner-linked NbO_6 octahedra within slabs parallel to [100]. The remaining two-thirds of the La ions are seven-coordinated and lie between the slabs of the LaO_8 and NbO_6 polyhedra.

The electronic and magnetic properties of the complex oxides containing pentavalent ruthenium ions attract our attention. The electronic configuration of Ru^{5+} ions is $[Kr]4d^3$ ([Kr] = krypton core). Such highly oxidized cations from the second transition series sometimes show quite unusual magnetic behavior. Van Berkel and Ijdo (3) first described Nd_3RuO_7 with space group $Cmcm$ as a superstructure of the cubic fluorite structure with $a_{orth} = 2a_{fluorite}$, $b_{orth} \approx c_{orth} \approx \sqrt{2}a_{fluorite}$ and suggested the same structure as that found for La_3NbO_7, determined from X-ray diffraction measurements. After that, Groen *et al.*, determined the precise structure (4). However, the physical properties of Ln_3RuO_7 have not been studied until very recently. Khalifah *et al.*, investigated electronic and magnetic properties of La_3RuO_7 through its neutron diffraction, electrical resistivity, and magnetic susceptibility measurements and band structure calculations (6). La_3RuO_7 is a semiconductor and it transforms to an antiferromagnetic state at $T_N = 17$ K. Frederick reported the magnetic properties of Pr_3RuO_7 (7). Pr_3RuO_7 is also antiferromagnetic below $T_N = 50$ K.

Here, we prepared two Ln_3RuO_7 (Ln = Sm, Eu) and have performed measurements for their magnetic, electrical resistive, Mössbauer spectroscopic, and thermal properties. The results will be discussed.

2. EXPERIMENTAL

As starting materials, Sm_2O_3(99.9%), Eu_2O_3(99.9%), and RuO_2(99.9%) were used. These reagents were obtained from Nihon Yttrium Co. Ltd. (for Sm_2O_3) and Soekawa Chemical Co. Ltd. (for Eu_2O_3 and RuO_2). They were weighed in appropriate metal ratios and the mixtures were ground in an agate morter, pressed into pellets and reacted in air at 1200°C for 48 h with several grindings.

X-ray powder diffractometry was carried out in the region $10° \le 2\theta \le 120°$ in increments of 0.02° (2θ) with a Rigaku MultiFlex using Cu$K\alpha$ radiation. The structures were refined with the Rietveld method, using the Rietan program (8).

The temperature dependence of the magnetic susceptibility was measured for Sm_3RuO_7 in the temperature region $2\text{ K} \le T \le 350\text{ K}$ and for Eu_3RuO_7 in the temperature

0022-4596/01 $35.00

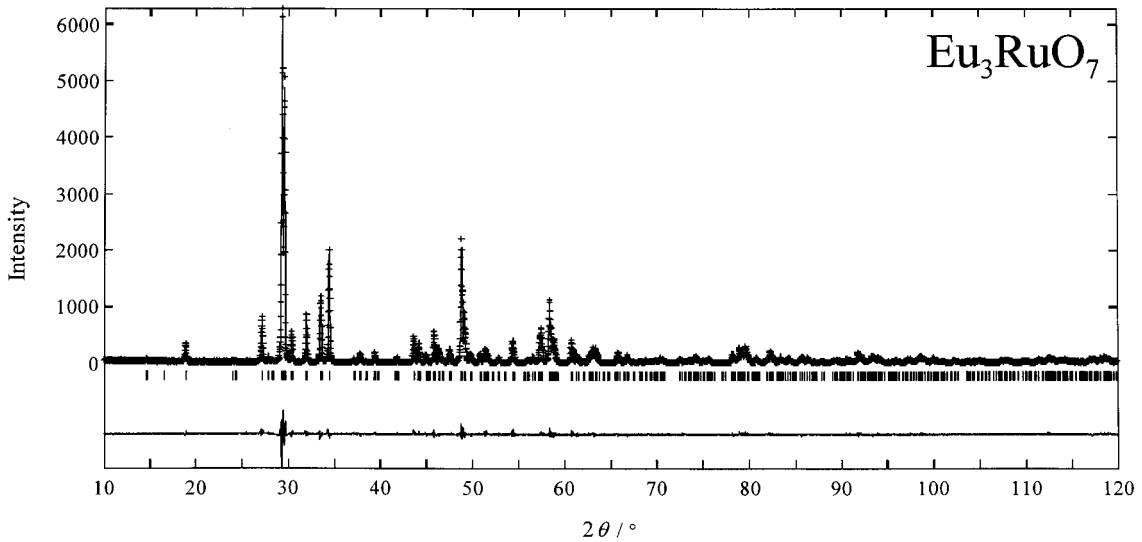

FIG. 1. X-ray diffraction profiles for Eu_3RuO_7. The calculated and observed diffraction profiles are shown on the top solid line and the cross markers, respectively. The vertical marks in the middle show positions calculated for Bragg reflections. The lower trace is a plot of the difference between calculated and observed intensities.

region $2\ K \leq T \leq 400\ K$ in a magnetic field of 0.1 T with a SQUID magnetometer (Quantum Design, Model MPMS). The magnetic susceptibility data were collected both after cooling the sample from room temperature to 2 K in a zero field (ZFC) and after cooling it in an applied field of 0.1 T (FC).

The temperature dependence of the resistivity of Eu_3RuO_7 was measured by the standard four-probe method in DC mode over the temperature range $150\ K \leq T \leq 400\ K$. The measurements of the specific heat were performed using a relaxation technique for Sm_3RuO_7 in the temperature range $1.8\ K \leq T \leq 350\ K$ and for Eu_3RuO_7 in the temperature range $1.8\ K \leq T \leq 400\ K$. The sample in the form of a pellet was mounted on an aluminum plate with apiezon for better thermal contact. Measurements of resistivity and specific heat were recorded with a Quantum Design PPMS.

The ^{151}Eu-Mössbauer absorption spectra for Eu_3RuO_7 were measured with a commercial transmissional Mössbauer spectrometer (VT-6000, Laboratory Equipment Co., Japan) at the temperatures 10, 50, and 260 K and RT. The spectrometer was calibrated using the magnetic hyperfine structure of α-Fe and the isomer shift was determined relative to the shift of europium trifluoride (EuF_3). $^{151}SmF_3$ with activity of 1.85 GBq was used as the γ-ray source.

3. RESULTS AND DISCUSSION

3.1. Crystal Structure

For both Sm_3RuO_7 and Eu_3RuO_7, the X-ray diffraction patterns were indexed on an orthorhombic unit cell (space group *Cmcm*). Figure 1 shows the X-ray diffraction profile for Eu_3RuO_7, as an example. No reflection forbidden for a *C* lattice was observed; i.e., the space group *Pnma* (La_3NbO_7) (9) or $P2_12_12_1$ (La_3MoO_7) (10) is not applicable to this case. This space group *Cmcm* is the same space group as that reported for other Ln_3RuO_7 (*Ln* = La, Pr, Nd). Their lattice parameters and atomic positions are listed in Table 1, and some important bond lengths and

TABLE 1
Crystal Structure Data for Ln_3RuO_7 (*Ln* = Sm, Eu)

Atoms	Positions	*x*	*y*	*z*	*B*(Å^2)
Sm_3RuO_7					
Space group *Cmcm*					
$Z = 4$ $a = 10.7552(2)$ Å $b = 7.3356(1)$ Å $c = 7.4375(1)$ Å $V = 586.79(2)$ Å^3					
$R_{wp} = 15.45\%$ $R_I = 2.68\%$ $R_F = 2.00\%$					
Sm(1)	4a	0	0	0	0.97(11)
Sm(2)	8g	0.2236(3)	0.3054(4)	0.25	0.48(7)
Ru	4b	0	0.25	0	0.32(13)
O(1)	16h	0.125(2)	0.317(3)	−0.040(2)	0.58(36)
O(2)	8g	0.129(3)	0.023(4)	0.25	0.58(36)
O(3)	4c	0	0.420(5)	0.25	0.58(36)
Eu_3RuO_7					
Space group *Cmcm*					
$Z = 4$ $a = 10.6927(1)$ Å $b = 7.3228(1)$ Å $c = 7.4125(1)$ Å $V = 580.40(1)$ Å^3					
$R_{wp} = 13.50\%$ $R_I = 2.24\%$ $R_F = 1.75\%$					
Eu(1)	4a	0	0	0	0.91(10)
Eu(2)	8g	0.2240(2)	0.3036(3)	0.25	0.27(6)
Ru	4b	0	0.25	0	0.25(10)
O(1)	16h	0.127(2)	0.316(2)	−0.039(2)	0.77(28)
O(2)	8g	0.130(2)	0.023(3)	0.25	0.77(28)
O(3)	4c	0	0.418(4)	0.25	0.77(28)

Note. Definitions of reliability factors R_{wp}, R_I, and R_F are given as follows $R_{wp} = [\sum w(|F(o)| - |F(c)|)^2/\sum w|F(o)|^2]^{1/2}$, $R_I = \sum |I_k(o) - I_k(c)|/\sum I_k(o)$, and $R_F = \sum |[I_k(o)]^{1/2} - [I_k(c)]^{1/2}|/\sum [I_k(o)]^{1/2}$.

TABLE 2
Bond Lengths and Angles for Ln_3RuO_7 (Ln = Sm, Eu)

Sm_3RuO_7			
Ru–O(1)	1.92(2) × 4	Sm(2)–O(2)	2.24(3)
Ru–O(3)	1.95(1) × 2	Sm(2)–O(2)	2.31(3)
		Sm(2)–O(1)	2.40(2) × 2
Sm(1)–O(1)	2.71(2) × 4	Sm(2)–O(1)	2.43(2) × 2
Sm(1)–O(2)	2.33(2) × 4	Sm(2)–O(3)	2.55(1)
Ave.(Sm(1)–O)	2.52	Ave.(Sm(2)–O)	2.39
Ru–O(3)–Ru	145.1(22)		
O(1)–Ru–O(3)	86.6(9)		
O(1)–Ru–O(1)	89.2(12)		
Eu_3RuO_7			
Ru–O(1)	1.93(2) × 4	Eu(2)–O(2)	2.24(2)
Ru–O(3)	1.95(1) × 2	Eu(2)–O(2)	2.28(2)
		Eu(2)–O(1)	2.38(2) × 2
Eu(1)–O(1)	2.70(2) × 4	Eu(2)–O(1)	2.40(2) × 2
Eu(1)–O(2)	2.32(2) × 4	Eu(2)–O(3)	2.54(1)
Ave.(Eu(1)–O)	2.51	Ave.(Eu(2)–O)	2.37
Ru–O(3)–Ru	144.0(17)		
O(1)–Ru–O(3)	85.9(7)		
O(1)–Ru–O(1)	89.4(9)		

angles are listed in Table 2. Figure 2 illustrates the crystal structure of Ln_3RuO_7 (Ln = Sm, Eu). In this structure, corner-shared RuO_6 octahedra form one-dimensional chain parallel to the c-axis. This chain is tilting not in the a-axis direction but in the bc plane, and has the mirror plane perpendicular to the a-axis existing center of it. Neighboring LnO_8 cubes and RuO_6 octahedroan share edges and are arranged alternately along the b-axis. The plane formed by the LnO_8 and RuO_6 is parallel to the bc plane and it is separated by the other lanthanum ions, $Ln(2)$, which have seven-fold coordination. The lattice parameters are determined: $a = 10.7552(1)$ Å, $b = 7.3356(1)$ Å, and $c = 7.4375(1)$ Å for Sm_3RuO_7, and $a = 10.6927(2)$ Å, $b = 7.3228(1)$ Å, and $c = 7.4125(1)$ Å for Eu_3RuO_7. With increasing atomic number of the lanthanide ions (which means decreasing ionic radius of Ln^{3+}), the lattice parameter decreases, as expected. The average seven-coordinated Eu–O and six-coordinated Ru–O lengths are 2.37 and 1.94 Å, respectively (see Table 2), which are very near to the values calculated from Shannon's ionic radii (2.39 and 1.945 Å). The average length for eight-coordinated Eu–O, 2.51 Å, is a little longer than that calculated from Shannon's ionic radii, 2.446 Å. These results indicate the bond lengths determined in this study are reasonable as the Eu–O and Ru–O bond lengths. The same result is found in the bond lengths for Sm_3RuO_7.

3.2. Specific Heat for Eu_3RuO_7

Figure 3 shows the temperature dependence of specific heat for Eu_3RuO_7. Two transition peaks are found at 22.5 and 280 K, respectively. The transition at lower temperature, 22.5 K is the λ-type second-order transition, indicating the occurrence of magnetic transition at this temperature. On the other hand, the shape of transition peak at higher temperature, 280 K, is characteristic of the first-order transition. And the variation of the specific heat with temperature is different below and above the transition temperature, which implies that the lattice component of specific heat changes at 280 K, indicating this transition is the structural phase transition. We will calculate the Debye temperature θ_D above 280 K by fitting the theoretical equation of lattice specific heat to the experimental data,

$$C_{\text{lattice}} = 9\,Nk_B\left(\frac{T}{\theta_D}\right)^3\int_0^{x_D} \mathrm{d}x\,\frac{x^4e^x}{(e^x-1)^2}. \qquad [1]$$

The Debye temperature is estimated to be $\theta_D = 520$ K. Now we can calculate the lattice contribution to the specific heat at $T = 280$ K, and then derive the entropy change, $\Delta S(T) = \int (C/T)\,\mathrm{d}T$. It is calculated to be $\Delta S = 4.32\ \mathrm{J\,mol^{-1}\,K^{-1}}$ from the C/T versus T curve.

3.3. Magnetic Susceptibility for Eu_3RuO_7

The temperature dependence of magnetic susceptibilities for Eu_3RuO_7 is shown in Fig. 4. It is found that Eu_3RuO_7 shows an antiferromagnetic transition at $T_N = 22.5$ K, in accordance with the specific heat data. The susceptibility increases rapidly when the temperature is decreased through ca. 24 K and a great divergence between the ZFC and FC magnetic susceptibility occurs at 22.5 K. The reciprocal susceptibility vs temperature curve shows the deviation from the Curie–Weiss law below 35 K. A short-range magnetic ordering between Ru^{5+} ions might be responsible for this deviation. In a very low-temperature region, the FC susceptibility has saturation value $\chi_M = 3.7\times10^{-1}$ emu mol^{-1} ($\mu = 6.6\times10^{-2}\,\mu_B$) and the ZFC susceptibility attains a constant value, $\chi_M = 1.4\times10^{-2}$ emu mol^{-1} ($\mu = 2.5\times10^{-3}\,\mu_B$). The electronic configuration of the Eu^{3+} ion in Eu_3RuO_7 is [Xe]$4f^6$ ([Xe]: xenon core). The ground state $^7F_0$ of Eu^{3+} is non-magnetic and the excited states ^7F_J are close enough to give energy differences comparable to k_BT (k_B, Bolzmann constant) at room temperature. Eu^{3+} has a magnetic moment due to the perturbation effect from these excited states. But this moment is very small. Therefore the magnetic ordering in the Eu_3RuO_7 should be due to the superexchange interaction between Ru^{5+} ions along the pathway of Ru–O–Ru. The Neél temperature for Eu_3RuO_7 ($T_N = 22.5$ K) is higher than that for La_3RuO_7 ($T_N = 17$ K), which is due to the increase of the orbital overlap of d_{z^2} (Ru^{5+}) and p_z (O^{2-}) in the Eu_3RuO_7. The Rietveld analysis for Eu_3RuO_7 and La_3RuO_7 show that the bond length of Ru–O(3) for

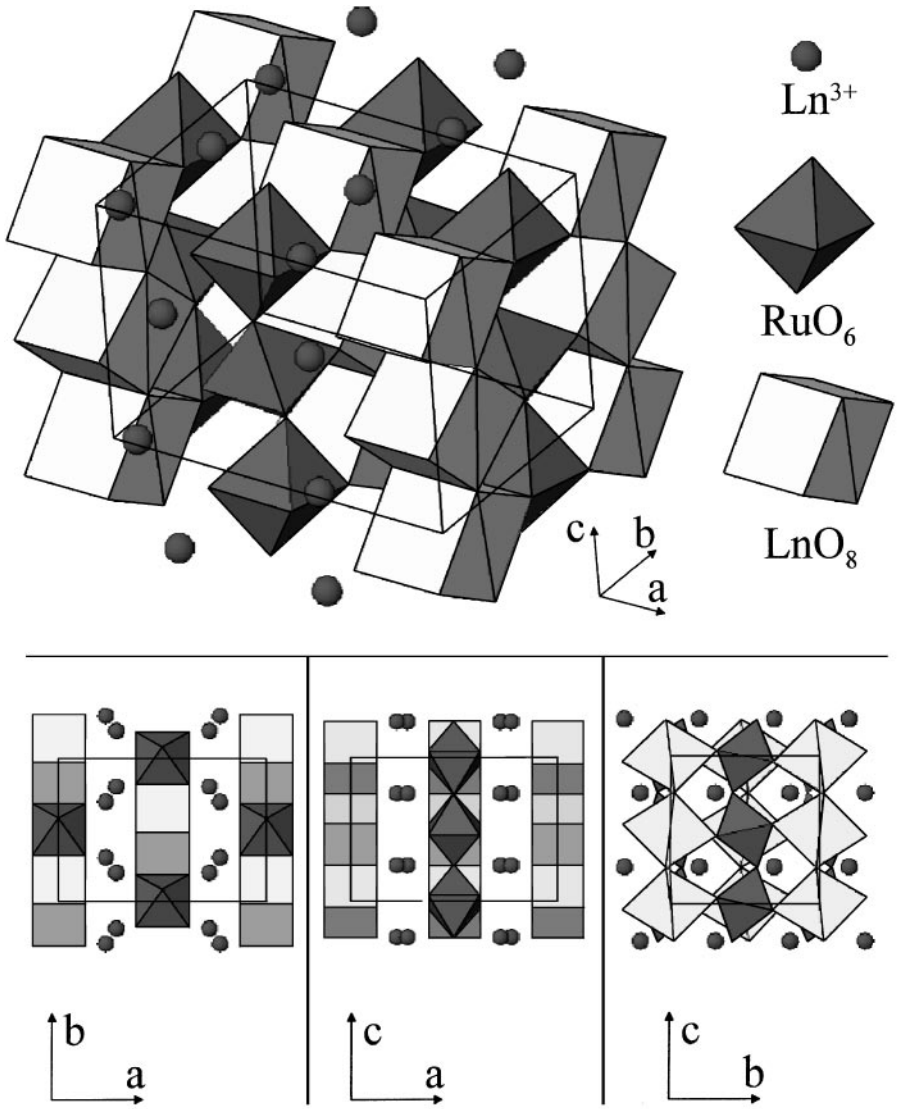

FIG. 2. The crystal structure of Ln_3RuO_7 (Ln = Sm, Eu).

Eu_3RuO_7 is certainly shorter than that for La_3RuO_7 (1.994(1) for La_3RuO_7, 1.95(1) for Eu_3RuO_7), although the bond angles of Ru–O(3)–Ru are not different between these two compounds (144.9(1)° for La_3RuO_7, 144.0(17)° for Eu_3RuO_7). Another possible reason for the high magnetic transition temperature of Eu_3RuO_7 is that the nonzero moments of Eu^{3+} ions might contribute to the magnetic exchange interactions.

Since the large divergence between the ZFC and FC susceptibilities for Eu_3RuO_7 was observed below the transition temperature, we have performed measurements of the field dependence of magnetization. A magnetic hysteresis loop has been observed, suggesting the existence of a ferromagnetic component in the magnetic moment of ruthenium. It is estimated to be $\mu = 7.1 \times 10^{-2}\ \mu_B$ from the remnant magnetization. When the magnetic field of 5 T is applied, the magnetic moment of Ru^{5+} is 0.41 μ_B, which is much smaller than the theoretical value $\mu = 3\mu_B$ in the case where all the Ru^{5+} moments are ferromagnetically arranged. We consider that this is due to the contribution of the weak ferromagnetic component. For compounds with low crystal symmetry having no inversion symmetry, a Dzyaloshinsky–Moriya (D–M) interaction can exist between the antiferromagnetically ordered moments, which results in the existence of a weak ferromagnetic component in the susceptibility (11). Since the Eu_3RuO_7 shows a very sharp peak in the magnetic susceptibility vs temperature curve at 22.5 K (see Fig. 4b), we can exclude the possibility that this magnetic interaction is of the one-dimensional Ising type, although the RuO_6 octahedra are arranged one-dimensionally in this structure.

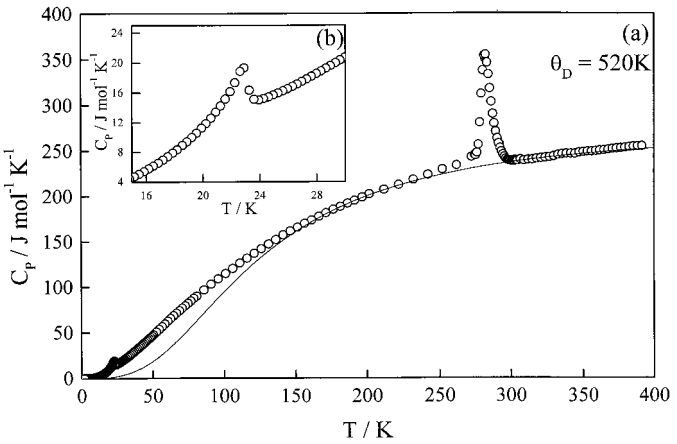

FIG. 3. Temperature dependence of specific heat of Eu_3RuO_7 in the temperature ranges, (a) $2\,K \leq T \leq 400\,K$ and (b) $15\,K \leq T \leq 30\,K$. The calculated lattice specific heat is shown with the solid line.

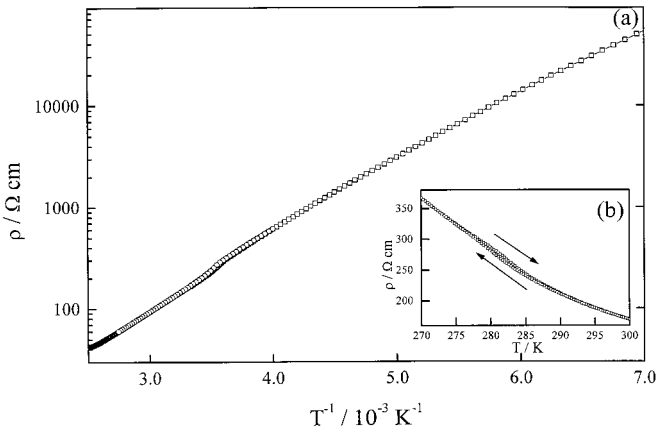

FIG. 5. Plots of electrical resistivity versus, (a) reciprocal temperature and (b) temperature plot for Eu_3RuO_7.

Detailed magnetic susceptibility measurements around 280 K show the slight magnetic anomaly in the susceptibility vs temperature curve (see Fig. 4c), which is in accordance with the results of specific heat measurements.

3.4. *Electrical Resistivity for Eu_3RuO_7*

In Fig. 5a, the electrical resistivity of Eu_3RuO_7, ρ, is plotted as a function of reciprocal temperature. The hysteresis loop is observed around 280 K (see Fig. 5b). At the same temperature, both the specific heat and the magnetic susceptibility show anomalies. But no jump of resistivity is observed and the resistivity is in the range for semiconductors throughout the measurements, as will be described below. Therefore, this transition is not a metal–insulator transition such as is observed, for example, for rare earth nickel perovskites $LnNiO_3$ (12, 13) or mixed valence manganese perovskites $A_{1-x}A'_xMnO_3$ (14).

The resistivity increase with decreasing temperature is found for semiconductors and it is 170 Ω cm at 300 K. From its Arrhenius plot, a band gap ΔE_g is estimated to be 0.25 eV in the temperature range $150\,K < T < 250\,K$ below the transition temperature, and $\Delta E_g = 0.26$ eV in the temperature range $310\,K < T < 400\,K$ above that temperature. These values are comparable to that reported for La_3RuO_7 ($\Delta E_g = 0.28$ eV), and suggesting that the d electrons of Ru^{5+} ions are localized. Considering the electronic configuration of the pentavelent ruthenium ion, $4d^3(t_{2g}^3, e_g^0)$, this compound is considered to be a Mott insulator.

3.5. *Mössbauer Spectra*

Figure 6 shows the Mössbauer spectra measured at room temperature in the velocity range $-10\,mm\,s^{-1} \leq v \leq 10\,mm\,s^{-1}$. As the structural analysis has indicated that the

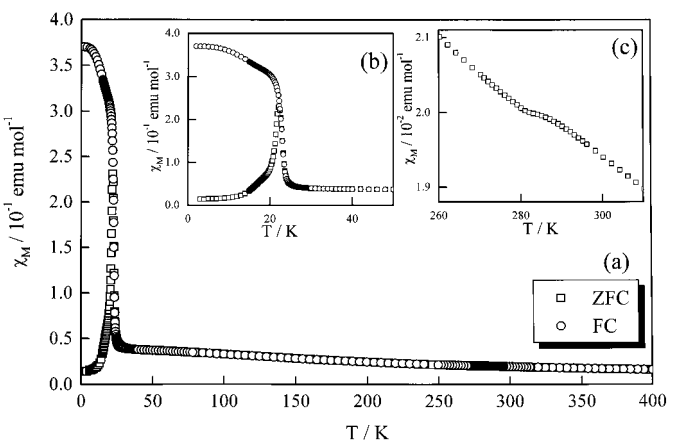

FIG. 4. Temperature dependence of magnetic susceptibilities of Eu_3RuO_7 in the temperature ranges, (a) $5\,K \leq T \leq 400\,K$, (b) $2\,K \leq T \leq 50\,K$, and (c) $260\,K \leq T \leq 310\,K$.

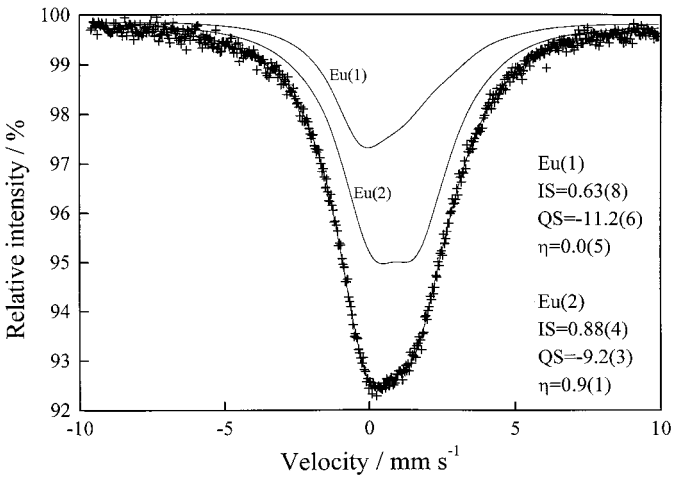

FIG. 6. The Mössbauer spectra for Eu_3RuO_7 in the velocity range $-10\,mm\,s^{-1} \leq v \leq 10\,mm\,s^{-1}$ at RT.

Eu ions occupy two kinds of sites, we assume two different environments for europium ions in analyzing the spectra. The ratio of their sites is Eu(1) : Eu(2) = 1 : 2.

First, we will discuss the isomer shifts (IS) determined in this study (see Fig. 6). The isomer shift δ is proportional to the difference in the probability density for the electrons at the nucleus of the absorber $\Psi_A(0)$ and the source $\Psi_S(0)$, and to the difference between the nuclear radii in the excited and the ground states ΔR, and it is given by

$$\delta \propto \{|\Psi_A(0)|^2 - |\Psi_S(0)|^2\} \times \Delta R. \qquad [2]$$

In the case of europium, the sign of ΔR is positive. Therefore, the IS increases with increasing electron density at the nucleus of absorber (at the sample). As the Eu–O bond length is shorter, its stronger covalency weakens the shielding effect of the 4*f* electron on the 6*s* orbital. Therefore, a negative linear relationship between the IS of Eu^{3+} and the Eu–O bond length has been reported for various oxides containing europium (15, 16). In this experiment the isomer shifts of Eu(1) and Eu(2) are determined to be 0.63(8) and 0.88(4) mm s^{-1}, respectively. Since the average bond length of Eu(1)–O (2.51 Å) is longer than that of Eu(2)–O (2.37 Å), the trend of the isomer shifts is in accordance with the above relationship. Since the Eu(1) and Eu(2) sites have the point symmetry 2/*m* and *m*, respectively, an electric field gradient (EFG) tensor exists, and we have to consider the effect of an electric quadrupole coupling $eV_{ZZ}Q$. The interaction between the EFG tensor and the electric quadrupole moment Q_g is described by the following Hamiltonian,

$$H_Q = \frac{eV_{ZZ}Q_g}{4I(2I-1)}[3I_z^2 - I(I+1) + \eta(I_x^2 - I_y^2)], \qquad [3]$$

where I is the nuclear spin, η is the asymmetric parameter, and V_{ii} is the electric field gradient tensor. The EFG tensor of principal direction, V_{ZZ}, is divided into two components; i.e., it is given by $V_{ZZ} = V_{\text{lattice}} + V_{4f}$, where V_{lattice} is the component of the contribution of the lattice, i.e., the crystal field formed from the coordinated oxygen ions, and V_{4f} is the component of the contribution of the 4*f* orbitals of the europium ions. The asymmetry parameter η is given by $\eta = (V_{yy} - V_{xx})/V_{zz}$. If the point symmetry of the europium site is lower than threefold symmetry ($-3m$), this parameter should be considered. Although some europium oxides containing distorted EuO_6 octahedra, such as monoclinic perovskites give positive quadrupole coupling constants (17, 18), most of europium oxides have negative values. In this study, $eV_{ZZ}Q$ is negative for both the sites Eu(1) and Eu(2) (see Fig. 6). The asymmetric parameters η for Eu(1) and Eu(2) are determined to be 0.0(5) and 0.9(1), respectively. The asymmetric parameter for Eu(2) is larger than that for Eu(1). This result is in accordance with the crystallographic result that the symmetry of the 7-coordinate site Eu(2) (point symmetry *m*) is lower than that of the 8-coordinate site Eu(1) (point symmetry 2/*m*).

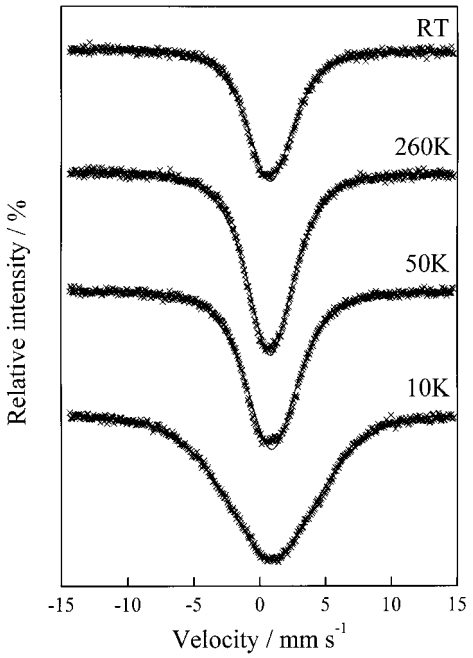

FIG. 7. The Mössbauer spectra for Eu_3RuO_7 in the velocity range $-15\ \text{mm s}^{-1} \le v \le 15\ \text{mm s}^{-1}$ at 10 K, 50 K, 260 K, and RT.

The large natural linewidth of the ^{151}Eu-Mössbauer spectrum ($\Gamma_{\text{nat}} = 1.31\ \text{mm s}^{-1}$) and the existence of two inequivalent sites in the crystal make the determination of its hyperfine structure difficult. In addition, because measurements of the temperature dependence of the ^{151}Eu Mössbauer spectra were carried out over the scanning velocity range between -15 and $15\ \text{mm s}^{-1}$, we could not fit the spectra with 12 Lorentzian because of the wide interval of the velocity. The results of the fitting with one Lorentzian for the Mössbauer spectra measured at various temperatures are shown in Fig. 7, and the isomer shifts (IS) and full widths at half-maximum (FWHM) are listed in Table 3. Both IS and FWHM increase with decreasing temperature. At 10 K, the spectra broaden greatly, indicating that a magnetic splitting occurs at this temperature. This result is in good agreement with the behavior found in the magnetic susceptibility and specific heat measurements below $T_N = 22.5$ K. The result that the IS increases with decreasing temperature is ascribable to the second-order Doppler shift with relativistic effects (19). This energy shift is described by the equation

$$\delta_D = -\frac{9k\theta_D}{MC}\left[\frac{1}{4} + 2\left(\frac{T}{\theta_D}\right)^4 \int_D^{\theta_D/T} \frac{x^3}{e^x - 1}\,dx\right], \qquad [4]$$

TABLE 3
Mössbauer Parameters of Eu_3RuO_7

	IS (mm s^{-1})	FWHM (mm s^{-1})
RT	0.80(1)	4.43(5)
260 K	0.81(1)	4.46(4)
50 K	0.91(1)	5.04(5)
10 K	0.93(1)	9.91(9)

where k is the Boltzmann constant, M is the atomic mass of europium, C is the speed of light, and θ_D is the Debye temperature. Substituting 520 K, estimated from the specific heat data for θ_D, we may obtain an energy shift $\delta_D = 0.0435$ mm^{-1} s between RT and 10 K. About 30% of the difference in isomer shifts between these temperature (0.13 mm s^{-1}) is due to the second-order Doppler shift. The rest of the difference should be attributable to the crystallographic result that Eu–O bond lengths become shorter with decreasing temperature, because there exists a negative relationship between the isomer shift and the Eu–O bond length, as described above.

3.6. *Magnetic Susceptibility and Specific Heat of Sm_3RuO_7*

Figure 8 shows the temperature dependence of magnetic susceptibility for Sm_3RuO_7. This Sm_3RuO_7 shows an antiferromagnetic transition at $T_N = 22.5$ K, and the divergence between ZFC and FC magnetic susceptibility has been obtained below this temperature. Its divergence is very larger when the temperature is decreased through 10.5 K (see Fig. 8b). Figure 9 shows the temperature dependence of specific heat for Sm_3RuO_7. It exhibits a sharp λ-type peak at 22.5 K and a broad anomaly appears in the temperature range below 10.5 K. These results are in good accordance

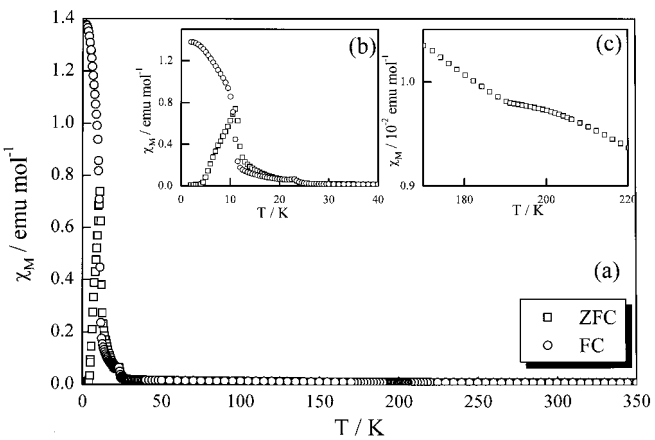

FIG. 8. Temperature dependence of magnetic susceptibilities of Sm_3RuO_7 in the temperature ranges, (a) 5 K $\leq T \leq$ 350 K, (b) 2 K $\leq T \leq$ 40 K, and (c) 170 K $\leq T \leq$ 220 K.

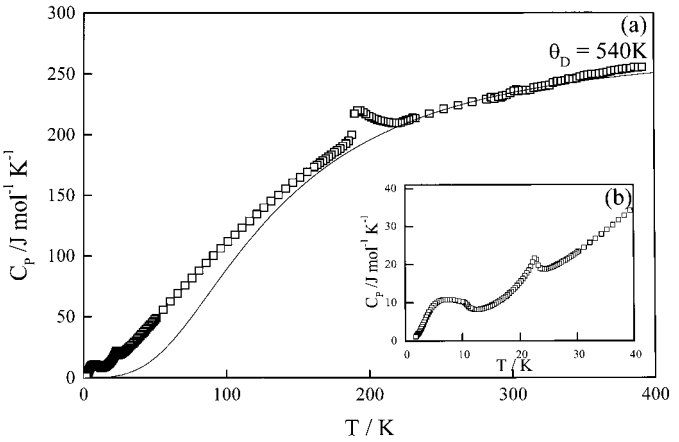

FIG. 9. Temperature dependence of specific heat of Sm_3RuO_7 in the temperature ranges (a) 1.8 K $\leq T \leq$ 400 K and (b) 1.8 K $\leq T \leq$ 40 K. The calculated lattice specific heat is shown by the solid line.

with magnetic susceptibility measurements. It is interesting that the antiferromagnetic transition temperature for Sm_3RuO_7 ($T_N = 22.5$ K) agrees with that for Eu_3RuO_7 ($T_N = 22.5$ K). This transition temperature is also near to that for La_3RuO_7 ($T_N = 17$ K). Therefore, we consider that these magnetic interactions are caused by the same interaction mechanism (between Ru^{5+} ions) and that they have no relation with the kinds of rare earth ions.

As shown in Fig. 9a, another specific heat anomaly has been found at 190 K. At the same temperature, the magnetic susceptibility also shows a small anomaly (see Fig. 8c). This behavior is quite similar to the case of Eu_3RuO_7, and we consider that this transition is also the structural phase transition. The Debye temperature for Sm_3RuO_7 is calculated to be $\theta_D = 540$ K by fitting Eq. [1] to the experimental data. After the component of lattice contribution is subtracted from the specific heat, the entropy change at $T = 190$ K is calculated to be $\Delta S = 2.46$ J mol^{-1} K^{-1}. This value is smaller than that for Eu_3RuO_7 ($\Delta S = 4.32$ J mol^{-1} K^{-1}).

3.7. *Evaluation of Specific Heat in Low-Temperature Regions of Sm_3RuO_7 and Eu_3RuO_7*

Figures 10a and 10b show the temperature dependence of magnetic entropy change and the magnetic specific heat divided by temperature (C_p/T) in the lower temperature region, respectively. Since the ground state $J = \frac{5}{2}$ of the Sm^{3+} ion is magnetic, the magnetic interaction between Sm^{3+} ions is also important in this Sm_3RuO_7. Thus we consider that the entropy change below 10.5 K, which is not found in Eu_3RuO_7, corresponds to an ordering of Sm^{3+} ions. Figure 11 shows the difference between the entropy change of Sm_3RuO_7 and that of Eu_3RuO_7. The entropy

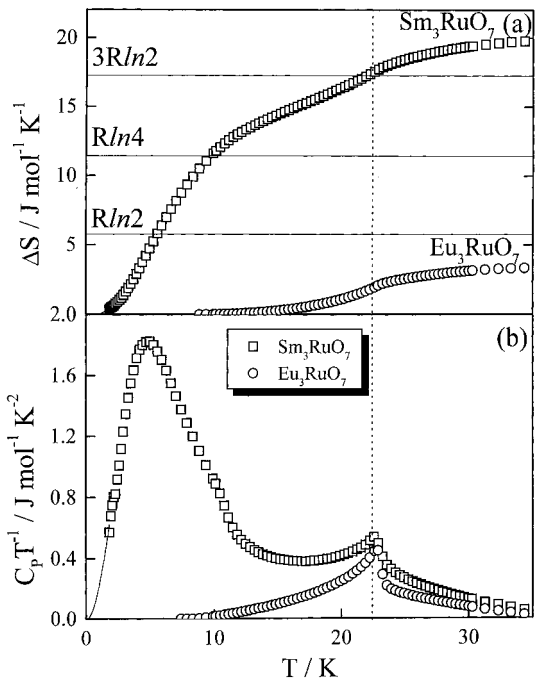

FIG. 10. (a) The magnetic entropy change versus temperature and (b) the C_p/T versus temperature for Ln_3RuO_7 (Ln = Sm, Eu).

curve is close to 16.5 J mol^{-1} K^{-1} with increasing temperature. We predict that this magnetic entropy is yielded by the ground Kramers' doublet of Sm^{3+} ions influenced by the crystal field. In the case where all three Sm^{3+} ions are ordered, the expected magnetic entropy is $3R\ln 2 =$ 17.3 J mol^{-1} K^{-1}, which is very close to the value obtained from measurements. As the magnetic entropy change attains about 75% of $3R\ln 2$ at $T = 10.5$ K, the ordering of magnetic moments for Sm^{3+} proceeds rapidly below this temperature.

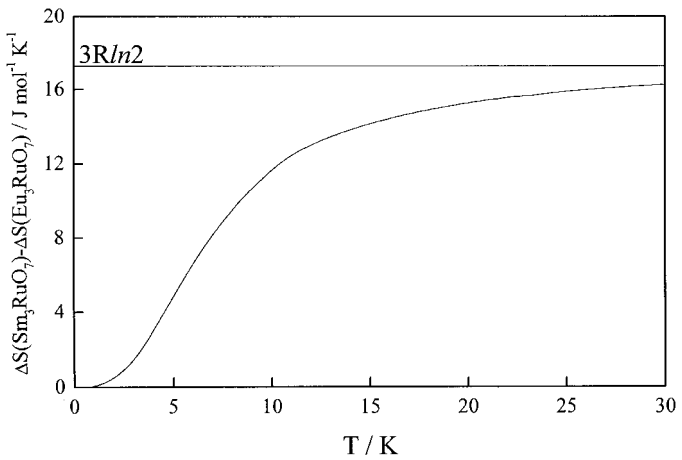

FIG. 11. The difference between the magnetic entropy of Sm_3RuO_7 and that of Eu_3RuO_7 as a function of temperature.

For Eu_3RuO_7 we have calculated the magnetic entropy change by subtracting the electronic and lattice contributions from the specific heat. It is known that the electronic and lattice contributions to the specific heat are proportional to the temperature and the third power of temperature, respectively. We evaluate the components of the electronic and lattice contributions by fitting the observed specific heat to the function $f(T) = a \times T + b \times T^3 + c \times T^5$ in the temperature ranges 1.8 K $< T <$ 3.0 K and 35 K $< T <$ 45 K, where little influence of magnetic transition is expected. The magnetic entropy change thus obtained is 3.3 J mol^{-1} K^{-1} (Fig. 10a). For the case of a total spin quantum number $S = \frac{3}{2}$ (for Ru^{5+}), the magnetic entropy is calculated to be $R\ln(2s+1) = R\ln(2\times\frac{3}{2}+1) = R\ln 4 =$ 11.5 J mol^{-1} K^{-1}. This result indicates that zero-field splitting of the spin states is caused by the magnetic anisotropy, as will be discussed below.

For the $S = \frac{3}{2}$, the effective Hamiltonian determining the ground spin state is described by the equation

$$H = \sum_i \{D[S_{iz}^2 - \tfrac{1}{3}S(S+1)] + E(S_{ix}^2 - S_{iy}^2)\}, \qquad [5]$$

where the constant values D and E are expressed using the second-order perturbation terms of the orbital component Λ_μ and the spin–orbital coupling parameter λ as follows: $D = -\lambda^2\{\Lambda_{zz} - \frac{1}{2}(\Lambda_{xx} + \Lambda_{yy})\}$ and $E = -\lambda^2(\Lambda_{xx} - \Lambda_{yy})/2$. Diagonalizing the energy matrix, this effective Hamiltonian makes four degenerating states split into two doublets, $|S = \frac{3}{2}, M_S = \pm\frac{3}{2}>$ and $|S = \frac{3}{2}, M_S = \pm\frac{1}{2}>$. The splitting energy ΔE is given by $\Delta E = 2[D^2 + 3E^2]^{1/2}$. Therefore the ground state should be a doublet, and the magnetic entropy change is calculated to be $R\ln 2$. This consideration almost explains the obtained small magnetic entropy change, but it is still smaller than $R\ln 2$. This may be due to the improper evaluation of the specific heat components other than the magnetic entropy one.

4. CONCLUSIONS

The ZFC magnetic susceptibility measurements for Eu_3RuO_7 show the antiferromagnetic transition at $T_N = 22.5$ K, which is due to the interactions between Ru^{5+} ions. ^{151}Eu-Mössbauer spectroscopic measurements and specific heat measurements also indicate the existence of the transition at 22.5 K. A large divergence between the ZFC and the FC magnetic susceptibilities below T_N indicates a weak ferromagnetic component in the magnetic moment of Ru^{5+}. For Sm_3RuO_7 a magnetic anomaly has been found at 10.5 K in addition to the magnetic transition at $T_N = 22.5$ K. We consider that the magnetic transition at

22.5 K is due to the interaction of Ru^{5+} ions, and that the magnetic anomaly at 10.5 K is ascribable to that of Sm^{3+} ions. The magnetic entropy change at 10.5 K for Sm_3RuO_7 suggests the ordering of Sm^{3+} ions. For samples of Sm_3RuO_7 and Eu_3RuO_7, the structural phase transitions are found at 190 and 280 K, respectively. The electric resistivity measurements for Eu_3RuO_7 show a hysteresis loop around 280 K, but no jump of resistivity occurs. This structural phase transition is not related to a metal–insulator transition.

ACKNOWLEDGMENT

This work was supported by Grant-in-Aid for Science Research on Priority Area "Novel Quantum Phenomena in Transition Metal Oxides —Spin · Charge · Orbital Couples Systems" No. 12046203 from the Ministry of Education, Science, Sports, and Culture of Japan.

REFERENCES

1. J. G. Allpress and H. J. Rossell, *J. Solid State Chem.* **27,** 105–114 (1979).
2. H. J. Rossell, *J. Solid State Chem.* **27,** 115–122 (1979).
3. F. P. F. van Berkel and D. J. W. Ijdo, *Mater. Res. Bull.* **21,** 1103–1106 (1986).
4. W. A. Groen, F. P. F. van Berkel, and D. J. W. Ijdo, *Acta Crystallogr. Sect. C* **43,** 2262–2264 (1986).
5. P. Khalifah, Q. Huang, J. W. Lynn, R. W. Erwin, and R. J. Cava, *Mater. Res. Bull.* **35,** 1–7 (2000).
6. P. Khalifah, R. W. Erwin, J. W. Lynn, Q. Huang, B. Batlogg, and R. J. Cava, *Phys. Rev. B* **60,** 9573–9578 (1999).
7. F. Wiss, N. P. Raju, A. S. Wills, and J. E. Greedan, *Int. J. Inorg. Mater.* **2,** 53–59 (2000).
8. F. Izumi, *in* "The Rietveld Method" (R. A. Young, Ed.), Chap. 13. Oxford Univ. Press, Oxford, 1993.
9. A. Kahn-Harari, L. Mazerolles, D. Michel, and F. Robert, *J. Solid State Chem.* **116,** 103–106 (1995).
10. J. E. Greedan, N. P. Raju, A. Wegner, P. Gougeon, and J. Padiou, *J. Solid State Chem.* **129,** 320–327 (1997).
11. Y. Doi and Y. Hinatsu, *J. Phys. Condens. Matter* **11,** 4813–4820 (1999).
12. P. Lacorre, J. B. Torrence, J. Ponnetier, A. I. Nazzol, P. W. Weng, and T. C. Huang, *J. Solid State Chem.* **91,** 225–237 (1991).
13. J. Perez, J. Gracia, M. Castro, J. Stanliewicz, M. C. Sanchez, and R. D. Sanchez, *J. Magn. Magn. Mater.* **196–197,** 541–542 (1999).
14. G. H. Rao, J. R. Sun, A. Kattwinkel, L. Haupt, K. Barner, E. Schmitt, and E. Gmelin, *Physica B* **269,** 379–385 (1999).
15. S. Tanabe, K. Hirao, and N. Soga, *J. Non-Cryst. Solids* **113,** 178–184 (1989).
16. A. Nakamura, N. Masaki, and M. Saeki, *Ceram. Trans.* **71,** 295–306 (1996).
17. M. Wakeshima, D. Harada, and Y. Hinatsu, *J. Solid State Chem.* **147,** 618–623 (1999).
18. K, Henmi, Y. Hinatsu, and N. Masaki, *J. Solid State Chem.* **148,** 353–360 (1999).
19. R. M. Housley and F. Hess, *Phys. Rev.* **146,** 517–526 (1966).